Development of a Probabilistic Trajectory Model for High-Altitude Scientific Balloons

Luke W. Renegar*
University of Maryland, College Park, MD 20742

High-altitude scientific balloons provide an accessible platform for investigating atmospheric phenomena and validating engineering technologies in demanding environmental conditions. To safely conduct ballooning operations, operators must consider the risk that their balloon will fly through restricted airspace or that the payloads will land in some impermissible, inconvenient, or otherwise undesirable location. Since high-altitude balloons are unguided, such assessment depends on accurate trajectory forecasting. This paper outlines the development of a new balloon trajectory model that uses Monte Carlo techniques to estimate the uncertainty in the balloon's landing location. The flight dynamics of high-altitude scientific balloons are discussed, as are uncertainties affecting a balloon's flight. The Monte Carlo-based method for propagating these uncertainties along the trajectory of the balloon is then presented.

Nomenclature

a	=	albedo	Subscripts:	=	
c	=	specific heat	∞	=	free-stream
el	=	solar elevation angle	g	=	lifting gas
g	=	acceleration due to gravity	f	=	canopy
m	=	mass	ca	=	convection with the atmosphere
v	=	velocity	cg	=	convection with the lifting gas
r	=	canopy radius	IR	=	infrared
r_{eff}	=	effective reflectivity	atm	=	atmosphere
z	=	altitude			
BC	=	ballistic coefficient			
C_d	=	drag coefficient			
F_b	=	buoyant force			
F_d	=	drag			
F_w	=	weight			
I	=	irradiance			
$\dot{Q}$	=	heat flux			
Re	=	Reynolds number			
R_e	=	Radius of the Earth			
T	=	temperature			
V	=	canopy volume			
α	=	absorptivity			
λ	=	longitude			
μ	=	dynamic viscosity			
ρ	=	density			
σ	=	Stefan-Boltzmann constant			
τ	=	transmissivity			
ϕ	=	latitude			

*Undergraduate Student, Department of Aerospace Engineering, 3179 Glenn L. Martin Hall. Student Member AIAA. lrenegar@umd.edu.

I. Introduction

HIGH-altitude scientific balloons are important tools for research and education. Consisting of a latex or plastic canopy that encloses a volume of lifting gas (hydrogen or helium), balloons provide a relatively simple, inexpensive platform to access the upper troposphere and lower stratosphere. Even the shortest balloon flights can last 90 minutes or more, significantly exceeding the duration of a sounding rocket flight, and certain balloons can stay aloft for several weeks at a time. Payloads suspend below the balloon are exposed to harsh conditions of less than 1% of sea-level atmospheric pressure and temperatures as much 70 K colder than on the ground.

One distinguishing characteristic of balloons is their limited, if not nonexistent, capability to control their trajectory. While planes and rockets rely on an active propulsion system and control surfaces to maneuver, balloons are passive. The ascent rate is controlled by the amount of lifting gas on board and the mass of the payload, while the horizontal motion is dictated by the wind. Even the most sophisticated balloon systems have only limited control over their trajectory, generally achieved by adjusting the shape of the canopy, venting lifting gas overboard, or jettisoning ballast. While such measures can influence the ascent or descent rate, they have little impact on the lateral motion.

This limitation of balloons makes *a priori* prediction of balloon trajectories a topic of considerable importance to balloon operators. At a minimum, knowing where the payload will land significantly expedites its recovery. Often, however, balloon operators are required to avoid flying through or landing in certain areas for safety or regulatory reasons [1]. Since the balloon cannot be diverted once launched, the operator must be confident prior to launch that the balloon will remain clear of undesirable locations. In order to make these determinations, operators rely on numerical trajectory models. While a significant body of literature exists on trajectory models for large, long-duration balloons, there has been limited research into models for short-duration latex balloons. This paper details the development of such a model, with particular emphasis on determining the effect of the various uncertainties on the landing location.

II. Physical Processes in Balloon Flight

In order to accurately predict a balloon's trajectory, it is necessary to understand the forces acting on it. Figure 1 presents a free-body diagram of a balloon in flight. There are three forces acting on the balloon: weight, buoyancy, and drag. Each is critical to understanding the balloon's trajectory.

The weight force on the balloon, F_w, is given by Eqn. 1.

$$\vec{F_w} = -m_{sys} g \hat{z} \tag{1}$$

The buoyant force on the balloon, F_b, which produces the balloon's lift, is given by Eqn. 2. It follows from Archimedes' Principle, which states that an object immersed in a fluid experiences an upward force equal to the weight of the displaced fluid. It is important to note that both the local density of the air and the volume of the balloon are dependent on the local atmospheric conditions, which in turn depend on the position and time.

$$\vec{F_b} = \rho_\infty V g \hat{z} \tag{2}$$

The final force on the balloon, drag, is the most complex. The drag force F_d is given by Eq. 3 [1, 2]. The drag force acts in all three directions and is responsible for both limiting the balloon's ascent velocity and coupling the balloon's horizontal motion with that of the wind. This latter effect comes from the fact that drag is most directly dependent on the balloon's velocity relative to the surrounding air, $\vec{v_{rel}}$, rather than its inertial velocity. Additionally, as will be described in the following sections, the balloon's cross-sectional area and coefficient of drag are functions of the balloon's state.

$$\vec{F_d} = -\frac{1}{2}\rho_\infty A_{top} |\vec{v_{rel}}| \vec{v_{rel}} \tag{3}$$

Since both the drag and buoyant forces depend on the size and shape of the balloon canopy, an accurate understanding of how the canopy behaves during flight is critical to effective trajectory prediction. Because the canopy is a flexible material that contains a gas, its behavior is closely related to that of the lifting gas, and both must be considered in order to get an accurate model.

A. Canopy Shape Model

A preliminary question in such an analysis is how to model the shape of the balloon. Large zero- and super-pressure balloons are typically made of multiple sheets of non-elastic material that are attached together, and they tend to assume a teardrop or pumpkin shape [3]. However, due to their elastic nature, smaller latex balloons tend to assume a shape

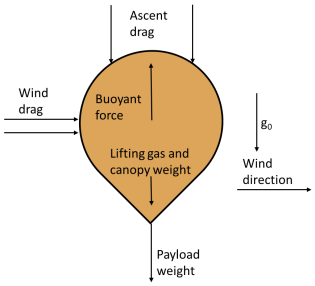

Fig. 1 Forces acting on a balloon in flight.

much closer to that of a sphere, albeit one distorted by the weight of the payloads suspended at the bottom. Despite this distortion, a spherical model is appropriate for latex balloons. Consider the balloon shown in Fig. 2, which is restrained prior to launch. As it is both restrained, which increases the tension in the payload line, and not fully expanded, causing less tension in the canopy than would be present at altitude, it presents a reasonable upper bound on non-sphericity. Image analysis shows that the spherical portion of the canopy (shaded red in Fig. 2) represents 86% of the cross-sectional area and 95% of the canopy volume, corresponding to less than a 2% error in radius. Since the canopy will be even more spherical at burst altitude, where canopy size and shape are even more critical than at launch, modeling the canopy as a sphere is a reasonable approximation.

Fig. 2 Latex balloon non-sphericity.

B. Canopy Volume Model

Determining the size of the canopy at a given point during the flight is a considerably harder problem, as it is continuously changing. It is most directly accomplished by applying the Ideal Gas law, $PV = mRT$, in combination with an initial measurement of the mass of the lifting gas. However, this method requires knowledge of the temperature and pressure inside the balloon across the entire flight envelope. Figure 3, based on data from Breeden [4], shows the temperature and pressure inside and outside a latex balloon canopy during flight. Although the elastic latex canopy does slightly compress the lifting gas, internal and external pressure remain within 1% of each other on average over the course of the flight, so treating the interior and exterior pressures as equal is reasonable. This is consistent with results from Conner [5]. The same cannot be said for temperature, however. The data show a significant (>30 K at some points) difference in interior and exterior temperature. This is perhaps to be expected, as the balloon is subject to appreciable radiative heating both from the Sun and from the Earth's surface [3]. It is thus necessary to construct a thermal model of the lifting gas.

C. Canopy and Lifting Gas Thermal Model

The thermal model presented here is modified from Farley [3], who derived a general thermal model for very large scientific balloons. Figure 4 displays the major heat transfer operations in effect on a balloon in flight. The upward

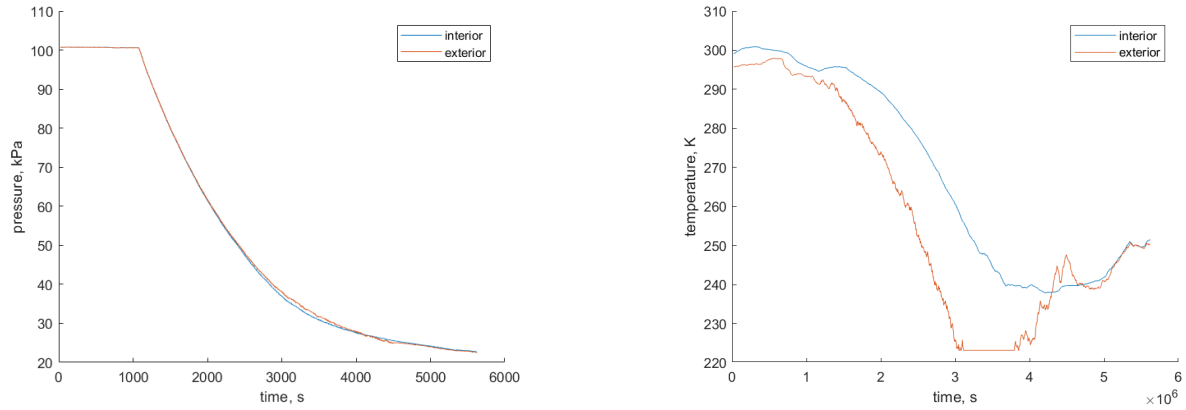

(a) Pressure vs. Time **(b) Temperature vs. Time**

Fig. 3 Comparison of temperature and pressure inside and outside the balloon canopy[4].

motion of the balloon forces convective transfer between the atmosphere and the canopy, and the canopy is radiatively heated by the Earth's surface, by direct sunlight, and by the sunlight reflected from the Earth (albedo). Heat transfer between the canopy and the lifting gas is by convection only, as the absorptivity of helium is negligibly small [1]. Because the canopy is extremely thin, temperature gradients across the canopy can be neglected [2].

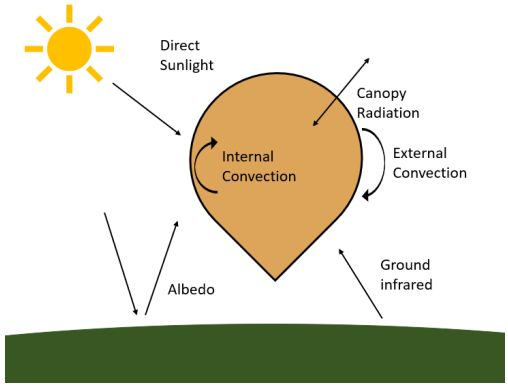

Fig. 4 Heat transfer processes acting on a balloon

Farley treats the canopy as one thermal mass of uniform temperature [3]. An alternative, presented by Lee [1], is to treat balloon as a tessellation of triangles and compute the various heat fluxes on each triangle individually. While this may be advantageous for very large balloons with complicated shapes, it is extremely expensive computationally, so implementing it on small, spherical latex balloons is difficult to justify. Adopting the model of a uniform canopy, the canopy temperature differential equation is given by Eqn. 4, which is nothing more than the sum of the heat fluxes on the canopy divided by its mass and specific heat capacity.

$$\frac{dT_g}{dt} = \frac{\dot{Q}_a + \dot{Q}_s + \dot{Q}_e + \dot{Q}_{ca} - \dot{Q}_{cg} - \dot{Q}_{IR}}{c_c m_c} \tag{4}$$

The gas temperature differential equation (Eqn. 5) is somewhat more complicated, accounting for adiabatic expansion of the lifting gas as well as convective transfer to the canopy [1, 3].

$$\frac{dT_g}{dt} = \frac{\dot{Q}_{cg}}{c_v m_g} + (\gamma - 1)\frac{T_g}{\rho_g}\frac{d\rho_g}{dt} \tag{5}$$

In the case that mass loss through the canopy is negligible, Eqn. 5 reduces to Eqn. 6. In order for a balloon to be an effective flight system, the rate of lifting gas diffusion must be relatively small, but little data exists to quantify this effect

[6]. However, other parts of the model must assume no lifting gas diffusion in order to remain computationally tractable, so it is assumed here as well.

$$\frac{dT_g}{dt} = \frac{\dot{Q}_{cg}}{c_v m_g} + (1-\gamma)\frac{T_g}{V}\frac{dV}{dt} \tag{6}$$

1. Radiative Transfer

Determining the magnitudes of each of the four radiative loads on the balloons requires reliance on numerous interrelated atmospheric and planetary science models. This section will present some of the more fundamental equations, but for a more in-depth treatment, the reader is referred to Farley and Lee [1, 3].

The solar flux at the top of Earth's atmosphere I_s is approximately 1.36 kW/m^2, but it varies seasonally with the Earth's distance from the Sun. The atmosphere absorbs some fraction of the incoming solar flux, so I_s must be multiplied by the atmospheric transmissivity, τ_{atm}, which is a function of altitude. The solar heating on the balloon's canopy is thus given by Eqn. 7 [3].

$$\dot{Q}_s = \alpha\pi r^2 \tau_{atm} I_s \left[1 + \tau\left(1 + r_{eff}\right)\right] \tag{7}$$

The balloon is subject to two radiative loads from the ground: the infrared radiation due to the ground temperature (Eqn. 9), and the reflection of the sun off the ground (albedo; Eqn. 10). In each case, the surface area with a direct view of the Earth is given by Eqn. 8 [3]. As with the direct sunlight, the altitude-dependent transmissivity of the atmosphere must be taken into account; this transmissivity is not the same for direct sunlight and infrared radiation.

$$A_{down} = 2\pi r^2 \left[1 - \sqrt{1 - \left(\frac{R_e}{R_e + z}\right)^2}\right] \tag{8}$$

$$\dot{Q}_{gr} = \alpha_{IR} A_{down} I_{gr} \tau_{atm,IR} \left[1 + \tau_{IR}\left(1 + r_{eff}\right)\right] \tag{9}$$

$$\dot{Q}_a = a\alpha A_{down} I_s \sin(el) \tau_{atm} \left[1 + \tau\left(1 + r_{eff}\right)\right] \tag{10}$$

The albedo factor a, which denotes the fraction of incident sunlight reflected by the Earth, varies significantly based on the terrain the balloon is flying over. Although Farley uses average albedo data [3], albedo accuracy can be significantly improved by relying on albedo data from the same numerical weather prediction sources that are used to provide data about the atmospheric state. While clouds can change the albedo reported from numerical models, federal regulations restrict the operation of balloons in cloudy environments [7], so this effect is of limited operational relevance.

The balloon's canopy also functions as an infrared emitter, radiating along both its inner and outer surfaces. Since the lifting gas does not absorb the radiation, some of it is re-absorbed by the canopy, either directly or after some number of internal reflections, while the rest is transmitted through to the atmosphere. The net effect of this radiative heat loss is given by Eqn. 11.

$$\dot{Q}_{IR} = 4\pi r^2 \sigma \alpha_{IR} T_f^4 \left[2 - \alpha_{IR}\left(1 + r_{eff}\right)\right] \tag{11}$$

2. Convective Transfer

In addition to the radiative loads, the canopy is subject to convective transfer with both the atmosphere (Eqn. 12) and the lifting gas (Eqn. 13). Determining the convection coefficient h_c in each case is beyond the scope of this paper; the reader is referred to references [3] and [8] for the relevant formulas.

$$\dot{Q}_{ca} = 4\pi r^2 h_{ca}(T_\infty - T_f) \tag{12}$$

$$\dot{Q}_{cg} = 4\pi r^2 h_{cg}(T_f - T_g) \tag{13}$$

D. Drag Coefficient Model

Drag on the balloon is given by Eqn. 3, which is dependent on the balloon's coefficient of drag C_d. For a sphere, C_d is strongly dependent on the Reynolds Number Re, given by Eqn. 14, where the ∞ subscript denote free-stream atmospheric conditions. It is important to note that the velocity is given relative to the atmosphere, so a balloon's horizontal movement with the wind does not affect the Reynolds number. Typical Reynolds numbers for latex balloon flights range from 50,000 to the single digit millions.

$$Re = \frac{2\rho_\infty v_\infty r}{\mu_\infty} \tag{14}$$

Figure 5 depicts the coefficient of drag for a sphere as a function of Reynolds number, using a relationships identified by Morrison and Conner [5, 9]. Morrison's model concerns spheres generally, while Conner's was developed specifically for latex balloons. As can be seen from Fig. 5, balloon flight Reynolds numbers span the region where the coefficient of drag decreases from 0.4-0.5 to 0.1 across a relatively narrow span of Reynolds numbers, referred to as the drag crisis. Because of the extreme variation in coefficient of drag in this region, the accurate modeling of the balloon's ascent rate requires that the C_d be treated as a function of Re. Conner's model was selected, as it is based on experimental data from latex balloon flights.

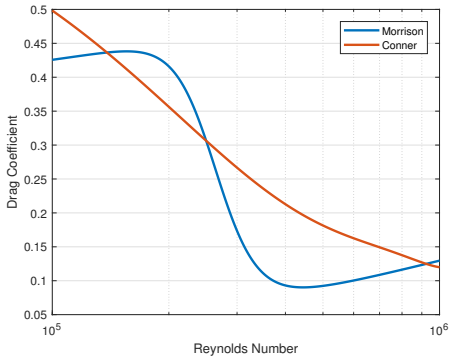

Fig. 5 Coefficient of Drag versus Reynolds Number for a Sphere.

E. Descent Under Parachute

Unlike in large scientific balloon flights, the descent of the payloads after canopy burst typically constitutes a significant portion of the flight time for latex balloon flights, and must be modeled in order to get an accurate landing site prediction. The only forces acting on the payloads under parachute are their weight and the drag force of the parachute. Video from balloon flights indicate that parachutes inflate to their full volume within a few seconds of the balloon bursting and remains so for the entire descent. Thus rather than trying to model the parachute area and coefficient of drag separately, they can be combined in a ballistic coefficient BC given by Eqn. 15. BC can be calculated based on the observed descent velocity of the system, either on a previous flight or during a drop test from a structure using Eqn. 16.

$$BC = \frac{C_d A_{parachute}}{m_{sys}} \tag{15}$$

$$BC = \frac{2g}{\rho_\infty v_\infty^2} \tag{16}$$

III. Equations of Motion

Now that a physical model of the balloon has been developed, it is possible to identify the balloon's equations of motion by applying Newton's Second Law, $\Sigma\vec{F} = m\vec{a}$. The results are given by Eqns. 17a-17c. It should be noted that the mass m_v appearing in these equations is not identically the system mass, but rather the system mass plus some

'added mass' of air that is dragged along with the balloon [10]; this combination is referred to as the 'virtual mass'. However, as will be shown in the following sections, these equations can be reduced to a form that eliminates m_v.

$$m_v \ddot{x} = \vec{F}_d \cdot \hat{x} \tag{17a}$$

$$m_v \ddot{y} = \vec{F}_d \cdot \hat{y} \tag{17b}$$

$$m_v \ddot{z} = (\vec{F}_d + \vec{F}_g + \vec{F}_b) \cdot \hat{z} \tag{17c}$$

A. Horizontal Equations of Motion

Equations 17a and 17b show that the balloon's horizontal velocity is dependent only on the drag force and the initial conditions. Because the drag force acts opposite the balloon's relative velocity with respect to the wind, it will act to drive the balloon's horizontal velocity to that of the wind. As an illustration of the time scales involved, Fig. 6 presents the results of simulating the release of a relatively large (5.5 kg payload) latex balloon in moderate conditions (wind at 4 m/s from the SSW). Both horizontal velocity components converge to the wind velocity within approximately 30 seconds; larger wind magnitudes would converge even faster. Since this time scale is relatively short compared to the 90+ minute flight lengths typical of latex balloons, it is a reasonable simplifying approximation to treat the balloon's horizontal velocity as identically equal to that of the surrounding air. As Sóbester notes, this assumption might be violated if the wind velocity changes drastically over a small altitude span, such as when entering or exiting the jet stream [6], but, unless released into severe weather, balloons are unlikely to spend more than a few minutes in such areas over the course of their flight.

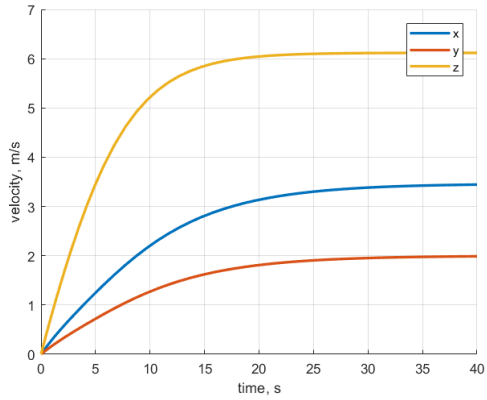

Fig. 6 Velocity Components vs. Time for a Balloon Released from Rest.

B. Vertical Equation of Motion

Equation 18 expands the vertical equation of motion (Eqn. 17c) under the assumption that there is no vertical wind and horizontal transients have settled.

$$m\ddot{z} = -\frac{1}{2}\rho_\infty A_{top} C_D \dot{z}.^2 - m_{sys} g + V\rho_\infty \tag{18}$$

Even though many of the variables on the right hand side of Eqn. 18 have a dependency on the state of the balloon, and thus time, $\dot{z}$ is the most time-dependent by at least an order of magnitude. Thus, locally, Eqn. 18 may be rewritten as an equation of the form $\ddot{z} = -A\dot{z}^2 + B$, with A, B constants. This form reveals that the balloon's ascent velocity $\dot{z}$ at any time will be locally asymptotic to some value. Since, as Fig. 6 shows, the balloon's velocity will rapidly return to this value when disturbed, it is appropriate to model the ascent velocity as a quasi-static process. Under this assumption, it is not necessary to integrate $\ddot{z}$, but rather $\dot{z}$ can be directly determined at each step from Eqn. 19, which was obtained by setting the left hand side of Eqn. 18 to 0 and solving for $\dot{z}$. This approach is consistent with with acceleration profiles calculated by Conner from balloon flight data, which show that latex balloons rarely experience maximum vertical acceleration magnitudes of more than 0.008 m/s^2, with typical values being less than 0.002 m/s^2 [5].

$$\dot{z} = \sqrt{\frac{2\left(\rho_\infty V g - m_{sys} g\right)}{\rho_\infty C_D A}} \tag{19}$$

IV. Numerical Implementation

The simplified kinematics presented in Section III were implemented using a fourth-order Runge-Kutta numerical integrator derived from Cambridge University's Tawhiri prediction engine [11], with the kinematic equations parameterized in the latitude-longitude-altitude frame. At each time step during ascent, the integrator sets the zonal and meridional velocities equal to the ambient wind velocity, calculates the ascent rate using Eqn. 19, and calculates dT_g/dt and dT_f/dt using the equations presented in Subsection II.C. The integrator compares the balloon's radius at the end of each time step to a specified burst radius, and uses this as the termination condition of the ascent. On descent, the descent velocity is calculated by inverting equation 16.

At each time step, it is necessary to obtain the ambient wind, temperature, and pressure, as well as the surface albedo and ground temperature of the sub-balloon point on the ground. These were extracted from the NOAA Global Forecasting System (GFS) model, which is a meteorological model with worldwide coverage at 0.5° spatial resolution and 3 hour temporal resolution. Variables are interpolated linearly in latitude, longitude, and time between grid points. Wind and temperature are also interpolated linearly with respect to altitude, while pressure is interpolated exponentially.

V. Characterization of Model Uncertainty

Any model of a physical process necessarily contains some uncertainty, as the model cannot capture all the details of the process. In balloon trajectory prediction, it is important to understand the degree to which the trajectory may deviate from the nominal prediction, as the key decision parameter for operators is the likelihood that the balloon will land in or pass through some undesirable location. This model attempts to quantify the effects of uncertainty in model through the use of Monte Carlo ensembles. By randomly deviating the input conditions across a large number of model runs, it is possible to develop a solution that shows where the balloon is most likely to land and the sensitivities of the trajectory to various input parameters. The model considers uncertainties that affect the balloon's ascent rate, horizontal drift, burst, and descent rate.

A. Ascent Rate Uncertainty

Equation 19 shows that the balloon's ascent rate is dependent on the ambient environmental conditions, the amount of lifting gas in the balloon, the system mass, and the coefficient of drag. Since small changes in temperature and pressure do not have a large effect on the balloon's ascent rate, uncertainty in these quantities is neglected in favor of modeling uncertainty in the system parameters.

The mass of the lifting gas can be measured indirectly at launch by measuring the lift at the neck of the balloon and subtracting the mass of the balloon's canopy. Experience has shown that this measurement can be rather imprecise due to the balloon being moved about by the wind. Since free lift is a fairly direct proxy for lifting gas mass, a normal distribution for lifting gas mass error is appropriate, as it reflects the underlying measurement uncertainty. Since the system mass that is not the lifting gas can be determined under laboratory conditions, its uncertainty can be considered negligible.

The drag coefficient is modeled as an explicitly function of Reynolds number, so it reflects the environmental uncertainties discussed above. However, since Conner's C_d model reflects an analytical curve fit, there is necessarily some additional uncertainty in the resulting value [5]. Additionally, the true C_d of the overall vehicle will reflect some drag on the payloads suspended below the balloon, which Conner's model does not account for. Since the C_d can vary by a factor of five or more over the course of the flight, and there is little reason to believe that significant perturbations exist that would be independent of Reynolds number, a multiplicative model of uncertainty seems more appropriate than an additive one. The model thus applies a unity-mean normally-distributed scale factor to the C_d from Conner's model, with a default standard deviation of 0.075.

B. Horizontal Drift

Since the balloon's horizontal motion is with the surrounding air, uncertainty in the wind model propagates directly to the balloon's trajectory. Because wind is an environmental uncertainty, wind perturbations are heavily correlated

spatially and temporally; if the wind deviates by a certain amount from the predicted value in one location, nearby locations will likely have a similar deviation. This problem is especially acute for the altitude axis, since the separation between points is much less than on the latitude and longitude axes [1]. Additionally, although the wind is parameterized in terms of zonal and meridional components, such a parameterization is somewhat arbitrary. As a result, the model should treat the uncertainties in zonal and meridional wind components as correlated.

In order to treat these correlations appropriately, the model generates two normally distributed values for each point in the latitude-longitude grid. The first value is a zero-mean angular deviation that is applied to the wind vector, with a default standard deviation of 5 deg. The second is a unity-mean multiplicative deviation that is applied to the wind velocity magnitude; this uncertainty has a default standard deviation of 0.05. Due to the strong correlation between wind at different altitude layers, the same deviations are applied for all points at the same latitude and longitude, regardless of altitude.

C. Burst Diameter Uncertainty

The burst diameter of the balloon determines the burst altitude, which, depending on the wind, can have a significant impact on the overall trajectory. Balloon manufacturers typically specify a nominal burst diameter for their balloons, but this is subject to considerable variation. The burst diameter is a measure of the balloon's lifetime, so a Weibull distribution is appropriate. The default parameter of $k = 14.4$ is taken from Sóbester's analysis of small latex meteorological balloons [6].

D. Descent Rate Uncertainty

In addition to the environmental uncertainties discussed in Subsection V.A, the descent rate is affected by uncertainty in the ballistic coefficient BC. This uncertainty is propagated through the Monte Carlo model as a normally-distributed unity-mean factor multiplying BC with a standard deviation of 0.05.

VI. Sample Model Output

Model output is plotted using the Google Maps API using code adapted from Tawhiri [11]. For Monte Carlo ensemble forecasts, the results can be plotted as a heat map, where warmer colors indicate a greater landing probability. Sample model output representing fairly typical balloon flight parameters is presented in Figs. 7 and 8, where the red bubble indicates the launch location. In Fig. 7, the prevailing wind is out of the southwest, so the landing site distribution is roughly ellipsoidal, with the major axis along the wind vector. The dominant operational uncertainty in the landing site is thus downrange distance. This distribution is quite typical of flights where the winds do not vary significantly in direction with altitude. Figure 8 depicts a situation where the wind changes from west to south with altitude. In this case, the landing site distribution is less one-dimensional, as the landing site is much more sensitive to ascent rate.

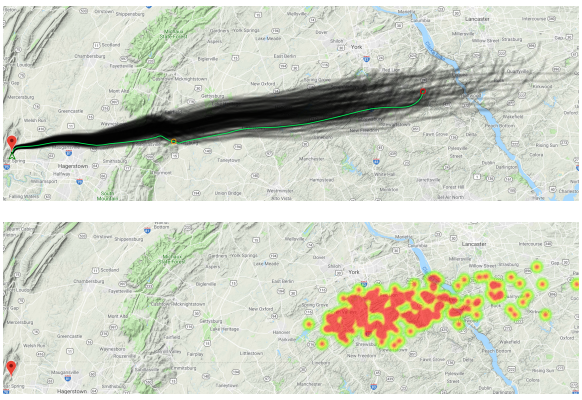

Fig. 7 Sample model output

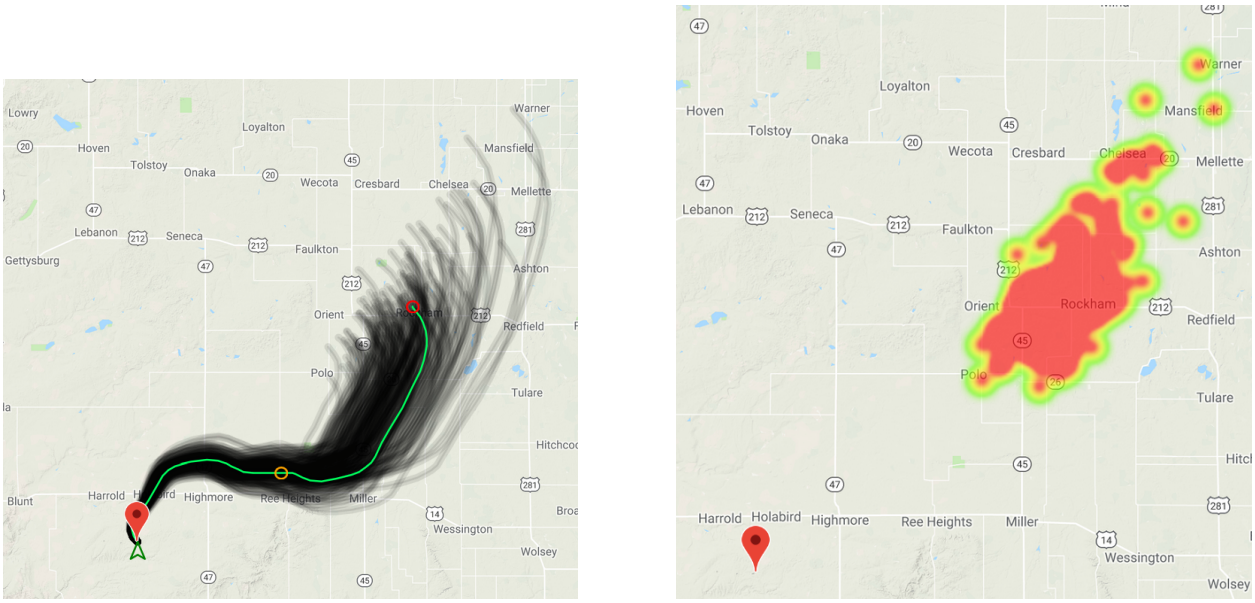

Fig. 8 Sample model output

VII. Conclusion

Effective prediction of scientific balloon trajectories is a topic of considerable importance to operators as it increases safety, simplifies planning, and helps ensure regulatory compliance. Because of the inherent uncertainty in balloon trajectory predictions, Monte Carlo models help operators understand the uncertainty in a trajectory prediction and make decisions accordingly.

In this paper, a general model of high-altitude scientific balloon trajectories has been developed. The balloon is treated as moving horizontally with the surrounding wind, while ascent is a function of canopy size and lifting gas density. Various convective and radiative transfer processes on the canopy are considered in order to accurately model the evolution of lifting gas temperature. The model supports Monte Carlo variation of fundamental simulation parameters in order to allow users to examine the effects of environmental and operational uncertainties. Sample model output is provided for different weather conditions experienced in operational environments. Verification of the model with flight data from the Balloon Payload Program at the University of Maryland is ongoing.

Acknowledgments

The author gratefully acknowledges the support of the Maryland Space Grant Consortium, Johns Hopkins University, and the National Aeronautics and Space Administration, whose funding of the University of Maryland Balloon Payload (UMDBPP) Program made this report possible. The author also acknowledges the support of the UMDBPP principal investigator, Dr. Mary Bowden, for her oversight of this paper, Michael Walker for his thoughts on balloon burst diameters, and Joseph Breeden for providing data about conditions inside the canopy.

References

[1] Lee, Y., and Yee, K., "Numerical Prediction of Scientific Balloon Trajectories While Considering Various Uncertainties," *Journal of Aircraft*, Vol. 54, No. 2, 2017, pp. 768, 782. doi:10.2514/1.C033998.

[2] Dai, Q., Fang, X., Li, X., and Tian, L., "Performance Simulation of High Altitude Scientific Balloons," *Advances in Space Research*, Vol. 49, 2012, pp. 1045, 1052.

[3] Farley, R., "Spacecraft Thermal Control, Design, and Operation," *AIAA Aviation, Technology, Integration, and Operations Conference*, Vol. 5, AIAA, 2005.

[4] Breeden, J., "High Altitude Weather Balloon Venting and Balloon Dynamics," *Region I Student Conference*, AIAA, 2017.

[5] Conner, J. P., and Arena, A. S., ""Near Space Balloon Performance Predictions"," *AIAA Aerospace Sciences Meeting*, Vol. 48, AIAA, 2010. doi:10.2514/6.2010-37.

[6] Sóbester, A., Czerski, H., Zapponi, C., and Castro, I., "High-Altitude Gas Balloon Trajectory Prediction: A Monte Carlo Model," *AIAA Journal*, Vol. 52, No. 4, 2014, pp. 832, 842. doi:10.2514/1.J052900.

[7] "14 C.F.R. 101.33," *Code of Federal Regulations*, n.d.

[8] Morris, A. L. (ed.), *"Scientific Ballooning Handbook"*, National Center for Atmospheric Research, 1975.

[9] Morrison, F. A., ""Data Correlation for Drag Coefficient for Sphere"," Tech. rep., 2016. URL `www.chem.mtu.edu/~fmorriso/DataCorrelationForSphereDrag2016.pdf`.

[10] Renegar, L., "A Survey of Current Balloon Trajectory Prediction Technology," *Academic High-Altitude Conference*, Stratospheric Ballooning Association, 2017.

[11] Richman, D., Greig, A., Patel, P., Judge, M., and Wareham, R., "Tawhiri," , 2016. URL `github.com/cuspaceflight/tawhiri`.